Available online at www.sciencedirect.com
ScienceDirect
International Journal of Heat and Fluid Flow 27 (2006) 777–788
International Journal of HEAT AND FLUID FLOW
www.elsevier.com/locate/ijhff

Interface conditions for hybrid RANS/LES calculations

A. Keating, G. De Prisco, U. Piomelli *

Department of Mechanical Engineering, University of Maryland, College Park, MD 20742, United States

Received 21 September 2005; received in revised form 3 March 2006; accepted 4 March 2006
Available online 19 June 2006

Abstract

Hybrid RANS/LES simulations, in which the attached boundary layers are computed using the Reynolds-averaged Navier–Stokes (RANS) equations, and the non-equilibrium regions of the flow by large-eddy simulation (LES), have received considerable attention over recent years. One issue that may affect (sometimes significantly) the accuracy of the results of hybrid methods is the generation from a smooth RANS field (in which the Reynolds stress is due entirely to the model) of turbulent eddies capable of supporting the Reynolds stresses in the LES region. In this paper, we perform hybrid RANS/LES of turbulent boundary-layer flows in zero, favorable and adverse pressure-gradients. The RANS equations are solved in regions of the flow that are at or near equilibrium, while LES is used elsewhere. Synthetic turbulence and controlled forcing are used to generate turbulent structures in the LES region. When only synthetic turbulence is used at the inflow of the LES region, some distance is required before the proper phase relationships between the modes introduced at the inlet are established; the turbulent statistics are unrealistic in this region, which can extend for 10–20 boundary layer thicknesses. When the forcing is used, this development region is significantly shortened, and realistic statistics are obtained 1–2 boundary-layer thicknesses downstream of the interface. The accuracy of the method, however, was found to depend critically on the accuracy of the RANS solution.

Keywords: Large-eddy simulation; Hybrid RANS/LES; Boundary-layer flows

1. Introduction

Hybrid RANS/LES simulations have received considerable attention over recent years due to their ability to apply the high accuracy of LES only in regions of the flow that demand it. In the typical application of these methods, a RANS calculation is carried out in regions where standard turbulence models are expected to be accurate (attached thin shear layers, for instance), while LES is used in non-equilibrium flow regions.

One issue that arises in these applications is the behavior of the flow in the transition zone between the RANS and LES regions. In the RANS zone the flow solution is either steady, or only contains information on the largest scales of motion if large-scale unsteadiness is present; most or all of the Reynolds shear stress is provided by the turbulence model. In the LES region, on the other hand, the resolved scales must supply most of the Reynolds shear stress and small scale structures must be present to provide it. Typically, a transition zone exists in which the resolved, energy-containing eddies are gradually generated and grow. The generation of realistic turbulent fluctuations at the RANS/LES interface is a critical factor in determining the length of this unrealistic transition region.

There are at least two ways to provide an interface condition in a hybrid calculation: a single grid can be used that spans the RANS and LES regions, and the eddies may be generated in the LES region either naturally, by the instabilities present in the flow [the approach followed in simulations of massively separated flows performed using DES (Spalart et al., 1997; Squires, 2004)], or by some form of stochastic forcing. The other technique involves the use of two separate computational domains, in which the

* Corresponding author. Tel.: +1 301 405 5254; fax: +1 301 314 9477.
E-mail address: ugo@eng.umd.edu (U. Piomelli).

0142-727X/$ - see front matter © 2006 Elsevier Inc. All rights reserved.
doi:10.1016/j.ijheatfluidflow.2006.03.007

RANS results are used to supply the statistics of the turbulence to be used as inflow for the LES. The latter approach is related to the specification of inflow conditions for LES, which generally uses one of three types of inflow boundary-conditions: random fluctuations superimposed on a mean profile; instantaneous velocity fields saved from a periodic, precursor simulation; or re-cycling and re-scaling a plane of velocity downstream of the inflow plane.

Within the framework of hybrid methods, the use of velocity fields obtained from a separate calculation is not feasible, since the flow in the RANS region cannot be computed by LES at a reasonable cost (otherwise there would be no reason for the use of hybrid methods). However, Schlüter et al. (2004) proposed an inflow boundary-condition for the LES region by re-scaling an instantaneous flow database saved from a separate calculation. The statistics of the flow database were rescaled based on the results of a RANS calculation in the upstream region. Simulations of confined swirling and non-swirling jets using this method yielded results in good agreement with experiments. It is unclear how the method would behave if the flow database were generated in conditions significantly different from those at the LES inflow.

The use of random fluctuations superimposed on a mean profile is also a feasible solution to the interface problem. The fluctuations (whose moments would be obtained from the RANS) could be either generated by localized forcing, or computed separately and superimposed on the random inflow profile, again obtained from the RANS. This approach, however, was found to require long transition distances for realistic turbulence to be generated (Le et al., 1997). More recent applications based on the synthetic, homogeneous turbulence generation method by Kraichnan (1970), which has been recently extended to inhomogeneous flows by Smirnov et al. (2001) and Batten et al. (2004), suffer from the same limitation Keating et al. (2004).

One inflow-generation technique that could be applied both to a single-grid calculation such as DES and to a method that uses the RANS data from a separate computation for the generation of the LES inflow was proposed by Spille-Kohoff and Kaltenbach (2001) and has been recently investigated by Keating et al. (2004). These studies showed that, by using synthetic turbulence at the inflow plane coupled with controlled forcing, the development length of the turbulent eddies could be substantially reduced. The forcing method enhances the velocity fluctuations at several control planes downstream of the inflow plane and is modulated so that a "target" Reynolds shear-stress profile is achieved. In those simulations, statistics calculated from an LES were used, so that the full Reynolds-stress tensor was available, as well as the dissipation rate; some of these statistics may not be available in a hybrid RANS/LES simulation.

In this paper, we perform more realistic hybrid simulations in which an LES region is appended to a RANS one, and the RANS statistical results (mean velocity profile and Reynolds shear stress, $\langle u'v' \rangle$) are used to supply the information required by the synthetic turbulence generation and controlled forcing methods discussed by Keating et al. (2004) to generate turbulent eddies for the LES. The hybrid calculations are compared to well-resolved LES of the entire domain. We examine more complex flows than those studied by Keating et al. (2004): in addition to the canonical zero-pressure-gradient boundary layer, we study flat-plate boundary layers in the presence of strong favorable and adverse pressure-gradients (denoted as FPG and APG, respectively). The latter include separation. In the following we first describe the governing equations, the numerical method, the synthetic turbulence generation and controlled-forcing algorithms, then present results for the three test-cases, and finally draw some conclusions.

2. Governing equations and numerical method

The governing equations for RANS and LES of an incompressible flow have the same form:

$$\frac{\partial \bar{u}_i}{\partial x_i} = 0 \tag{1}$$

$$\frac{\partial \bar{u}_i}{\partial t} + \frac{\partial \bar{u}_j \bar{u}_i}{\partial x_j} = \frac{1}{Re}\frac{\partial^2 \bar{u}_i}{\partial x_j \partial x_j} - \frac{1}{\rho}\frac{\partial \bar{p}}{\partial x_i} - \frac{\partial \tau_{ij}}{\partial x_j} + f_i \tag{2}$$

where overbars indicate the Reynolds-averaged quantities (in the RANS region) and filtered quantities (in the LES region), and the last term on the right-hand-side of (2) is the forcing that will be described later. In both regions an eddy-viscosity model is used to close the above set of equations:

$$\tau_{ij} - \frac{\delta_{ij}}{3}\tau_{kk} = -2\nu_t \bar{S}_{ij}. \tag{3}$$

The Spalart–Allmaras one-equation turbulence model (Spalart and Allmaras, 1994) is used to calculate ν_t in the RANS region, while in the LES region, the Lagrangian dynamic eddy-viscosity model is used (Germano et al., 1991; Meneveau et al., 1996).

The governing equations were solved on a Cartesian staggered grid. Conservative second-order finite differences were used for spatial discretization while a fractional-step method (Kim and Moin, 1984) coupled with a second-order implicit Crank–Nicolson method (for the wall-normal diffusion term) and a third-order explicit Runge–Kutta method (for the remaining terms) was used for time integration.

2.1. Synthetic turbulence generation

The synthetic turbulence generation method of Batten et al. (2004) is used to create a three-dimensional, unsteady velocity field at the inflow plane of the LES region. An intermediate velocity, v_i is first constructed, using a sum of sines and cosines with random phases and amplitudes:

$$v_i(x_j, t) = \sqrt{\frac{2}{N}} \sum_{n=1}^{N} \left[p_i^n \cos(\hat{d}_j^n \hat{x}_j^n + \omega^n \hat{t}) + q_i^n \sin(\hat{d}_j^n \hat{x}_j^n + \omega^n \hat{t}) \right], \tag{4}$$

where

$$\hat{x}_j = 2\pi x_j/L_b, \qquad \hat{t} = 2\pi t/\tau_b \tag{5}$$

are spatial coordinates normalized by the length- and time-scale of the turbulence. In the above, $\tau_b = k/\varepsilon$ and $L_b = \tau_b/V_b$ are the turbulence time- and length-scale, and $V_b = k^{1/2}$ is the velocity scale.

The random frequencies $\omega^n = N(1,1)$ in Eq. (4) are taken from a normal distribution $N(\mu,\sigma^2)$ with mean $\mu = 1$ and variance $\sigma^2 = 1$. The amplitudes are given by

$$p_i^n = \epsilon_{ijk}\zeta_j^n d_k^n, \qquad q_i^n = \epsilon_{ijk}\xi_j^n d_k^n, \tag{6}$$

where $\zeta_i^n,\ \xi_i^n = N(0,1)$, and

$$\hat{d}_j^n = d_j^n \frac{V}{c^n} \tag{7}$$

are modified wavenumbers obtained by multiplying the wavenumbers, d_i^n, by the ratio of the velocity scale $V_b = L_b/\tau_b$ to c^n, given by

$$c^n = \sqrt{\frac{3}{2}\langle u_l' u_m'\rangle \frac{d_l^n d_m^n}{d_k^n d_k^n}}. \tag{8}$$

The wave-numbers $d_i^n = N(0,1/2)$ are chosen from a normal distribution with variance 1/2, resulting in a three-dimensional spectrum that behaves like $d^4\exp(-d^2)$. In the original proposal by Batten et al. (2004), c^n was used to elongate those wavenumbers that are most closely aligned with the largest component of the Reynolds-stress tensor.

In the present work, the Spalart–Allmaras model is used for the RANS section of the domain, the results of which are used to provide the input parameters for the synthetic turbulence; therefore neither the turbulent kinetic energy (TKE), k, nor the dissipation rate ϵ, are available. We use an experimental correlation (Bradshaw et al., 1967; Townsend, 1962) to relate the TKE, k, to the Reynolds shear stress, $\langle u'v'\rangle$, which is available from the RANS solution:

$$|-\langle u'v'\rangle| = v_t\left|\frac{\partial u}{\partial y}\right| = a_1 k; \tag{9}$$

here $a_1 = \sqrt{c_\mu}$ and $c_\mu = 0.09$. To approximate the dissipation, we use the definition of eddy-viscosity from the k–ϵ turbulence model to express ϵ in terms of k and v_t (Menter, 1997):

$$\epsilon = c_\mu k^2/v_t. \tag{10}$$

These approximations were found to agree reasonably well with the values of k and ϵ calculated from a periodic LES. Furthermore, the SA model does not give information on the individual normal components of the Reynolds stress tensor; for this reason, they are assumed to be equal:

$$\langle u'u'\rangle = \langle v'v'\rangle = \langle w'w'\rangle = \frac{2}{3}k. \tag{11}$$

Keating et al. (2004) observed that, in plane channel flow, this assumption does not affect the results of the forcing very much. It is conceivable, however, that more sophisticated Reynolds-stress models that do not require this assumption would yield improved results in flows in which the RANS region is more strongly anisotropic. As a consequence of this assumption, the wavenumbers $\hat{d}_j^n$ used in the present formulation are also isotropic.

The synthetic turbulent fluctuation field is finally reconstructed by a tensor scaling:

$$u_i' = a_{ik}v_k. \tag{12}$$

Here a_{ik} is the Cholesky decomposition of the Reynolds-stress tensor.

In the simulations presented here, the number of modes, N, used to generate the synthetic field was 200. This number was required to ensure that the resulting statistics were independent of the number of modes used. Further details of the method can be found in Batten et al. (2004).

2.2. Controlled forcing

The controlled-forcing method proposed by Spille-Kohoff and Kaltenbach (2001) adds a forcing term to the wall-normal momentum equation that amplifies the velocity fluctuations in that direction, thus enhancing the production term in the shear-stress budget. As discussed in Spille-Kohoff and Kaltenbach (2001) and Keating et al. (2004), the forcing aims to enhance (or damp) local flow 'events' (bursts and sweeps) that contribute to the Reynolds shear stress $\langle u'v'\rangle$. Enhancing the v' fluctuations also has the effect of accelerating the production of Reynolds shear stress, which, in zero-pressure-gradient boundary-layer flows, is given by

$$P_{uv} = \langle v'v'\rangle\frac{\partial U}{\partial y}. \tag{13}$$

In more complex flows (even in the accelerating or decelerating boundary layers examined here) other mechanisms of shear-stress production may become important, and more sophisticated forcing mechanism may need to be developed. This work is, however, beyond the scope of the present paper.

Notice, furthermore, that the velocity correction step implicitly applies the projection operator to the force as well as to the velocity, and makes it divergence-free.[1] This effectively redistributes the force between the three velocity components.

A controller is used to determine the forcing amplitude based on the error in the Reynolds shear-stress:

$$e(y,t) = \langle u'v'\rangle^*(x_o,y) - \langle u'v'\rangle^{z,t}(x_o,y,t), \tag{14}$$

[1] Simulations were performed making the force divergence-free explicitly before adding it to the RHS of the momentum equation, with identical results to those presented here. Note that the resulting velocity field is always divergence-free, since the force is added before the projection step in the fractional step method, and simulations with the explicit divergence-free projection of the force are somewhat more expensive due to the need for an additional Poisson equation solution.

where $\langle u'v'\rangle^*(x_o, y)$ is the target Reynolds shear stress at the control plane $x = x_o$ (which here is obtained from the RANS solution), and $\langle u'v'\rangle^{z,t}(x_o, y, t)$ is the current Reynolds shear stress, averaged over the spanwise direction and time using an exponential window with a time-constant equal to $0.05 - 0.1\delta/u_\tau$. The force magnitude is set to

$$f(x_0, y, z, t) = r(y, t)\left[u(x_0, y, z, t) - \langle u\rangle^{z,t}(x_0, y)\right], \tag{15}$$

where f is related to the error by

$$r(y, t) = \alpha e(y, t) + \beta \int_0^t e(y, t')\mathrm{d}t' \tag{16}$$

The integral part of the controller has the effect of reducing the response of the forcing to very sharp changes which could make the system unstable. The constants α and β were chosen by Spille-Kohoff and Kaltenbach (2001) in such a way as to decrease the error rapidly, without causing instabilities. The values used in that paper and in our previous simulations (Keating et al., 2004), were $\alpha = 1$ and $\beta = 1$. We subsequently found that the transient period for the controllers could be significantly reduced (without adverse effects on other parameters) by increasing β to 30. All the simulations presented in this paper, therefore, were carried out with $\alpha = 1$ and $\beta = 30$. Further details on the forcing method may be found in Spille-Kohoff and Kaltenbach (2001) and Keating et al. (2004).

3. Applications

3.1. Zero-pressure gradient boundary layer

Initial simulations were performed for a zero-pressure gradient turbulent boundary layer. Three simulations were carried out: a full-domain LES (domain size: $240\delta_0^* \times 25\delta_0^* \times 25\delta_0^*$, where δ_0^* is the displacement thickness at the inflow), and two hybrid RANS/LES calculations. The full-domain LES with this grid agrees well with experimental and DNS data (for a full validation of the LES data, see, for instance, Keating and Piomelli, 2004). In the hybrid cases, the RANS equations were solved using the Spalart–Allmaras model in a domain with dimensions $(150\delta_0^* \times 25\delta_0^* \times 25\delta_0^*)$; at $x/\delta_0^* = 80$ an LES domain, of dimensions $120\delta_0^* \times 25\delta_0^* \times 25\delta_0^*$ began. The control planes were distributed over a length of $25\delta_0^*$ downstream of the RANS/LES interface. A full RANS calculation that used the Spalart–Allmaras model (referred to as "SA-RANS") was also performed for comparison. See Fig. 1 for a sketch of the computational configurations.

The inflow Reynolds number (based on freestream velocity and displacement thickness) was $Re_\delta^* = 1000$. The grid spacings in the streamwise and spanwise directions were $\Delta x/\delta_0^* = 1.25$ and $\Delta z/\delta_0^* = 0.385$, while 64 points were used in the wall-normal direction (with $y_{\min}^+ \approx 1.0$). The recycling and re-scaling method of Lund et al. (1998) was used at the inflow of the reference LES and RANS. Data from the RANS solution in the overlapping region was used for the generation of the synthetic turbulence in the LES region of the hybrid calculation, and also as the target profile for the controlled forcing.

Fig. 2 shows the coefficient of friction, $C_f = \tau_w/(\rho U_\infty^2/2)$ and the integrated Reynolds shear stress, $\int_0^\infty \langle u'v'\rangle(y)\mathrm{d}y$, as a function of downstream distance. The shaded region indicates the area in which the controlled forcing is used. First note that the RANS and full-domain LES solutions differ, even in this simple case of a zero-pressure gradient boundary layer. This difference (in particular the differences in C_f) is caused by a combination of the relatively low resolution of the LES and the low Reynolds number affecting the

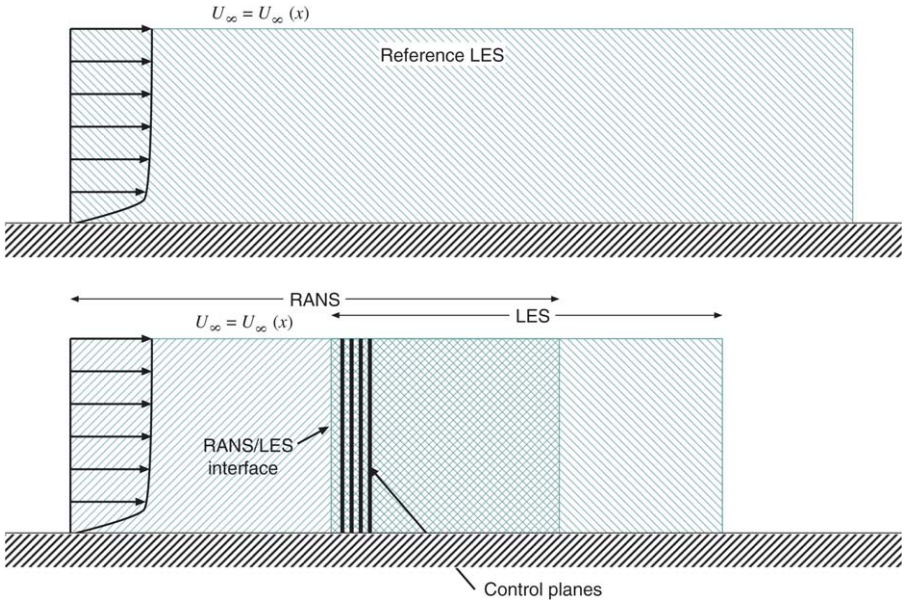

Fig. 1. Sketch of the numerical configurations.

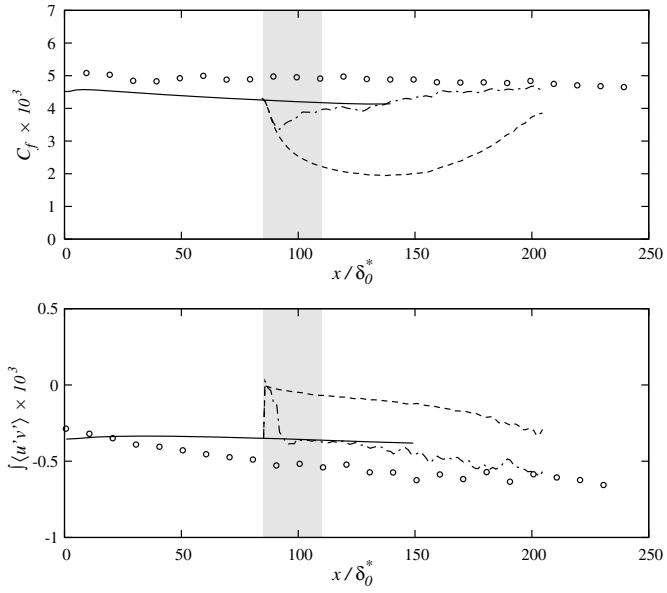

Fig. 2. Zero-pressure-gradient boundary layer. Coefficient of friction and integrated Reynolds shear stress. (○) Full domain LES; (—) SA-RANS solution; (----) hybrid, LES solution with synthetic turbulence at interface; (-·-) hybrid, LES solution with synthetic turbulence and forcing at the interface. The forcing is applied in the shaded region.

Spalart–Allmaras turbulence model. This poses a difficulty in matching the RANS and LES solutions at the interface, and therefore a transition region in which the flow adjusts from the RANS solution towards the LES one is observed.

When only synthetic turbulence is used at the RANS/LES interface, the flow undergoes a laminarization process downstream of the interface, and C_f does not reach the levels obtained in the full-domain LES before the end of the domain. This behavior was discussed in the context of channel flow calculations by Keating et al. (2004). When controlled forcing is used, the flow quickly recovers to the RANS value, then slowly adjusts to the LES level. Notice that, in a practical RANS/LES application, the LES results would not be realistic in the region where the forcing is applied; in this area, the RANS results must still be accurate. After $x/\delta_0^* \approx 120$, however, the LES results become accurate.

Mean velocity profiles and profiles of $q^2 = \langle u_i' u_i' \rangle$ (the resolved part of the trace of the Reynolds-stress tensor) are shown in Fig. 3 at $x/\delta_0^* \approx 130$ and 180. Without the controlled forcing, the flow tends to re-laminarize. However with the introduction of the controlled forcing, the re-laminarization is quickly reversed, and the mean velocity profile shows relatively good agreement with the RANS at the end of the transition region, and slowly approaches the full-domain LES results. The profiles of q^2 show a similar behavior. Note the low levels of q^2 at the edge of the boundary layer in the hybrid calculation, caused by the slow, wall-outward re-development of turbulence, a phenomenon also observed in previous simulations (Keating et al., 2004).

3.2. Favorable-pressure-gradient boundary layer

To investigate the performance of the RANS/LES interface in a non-equilibrium flow, simulations of a boundary layer subjected to a favorable pressure-gradient (FPG) were performed. In this flow, if the acceleration is rapid enough, re-laminarization and re-transition of the flow

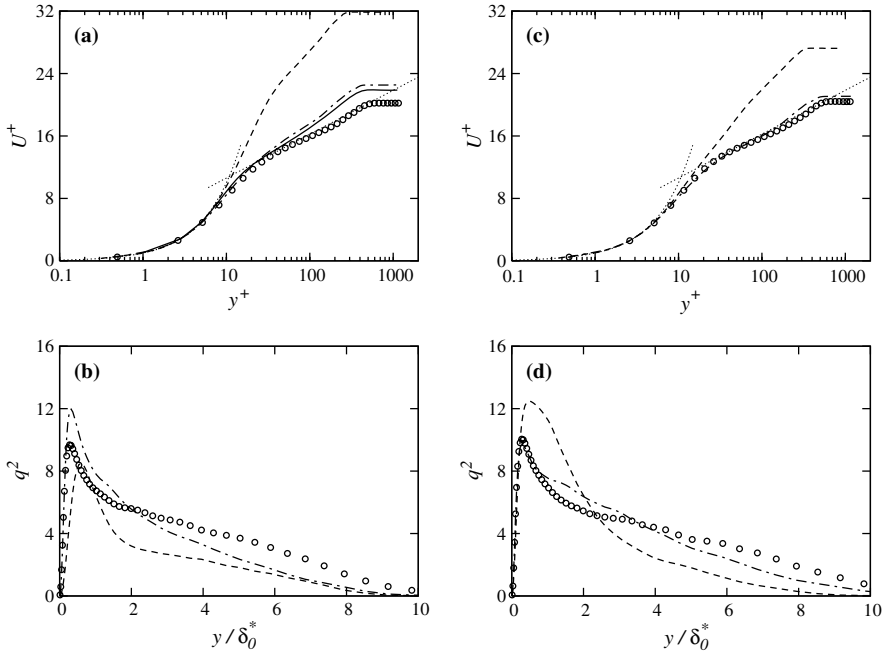

Fig. 3. Zero-pressure-gradient boundary layer: mean velocity and q^2 profiles at $x/\delta_0^* \approx 130$ (a,b) and $x/\delta_0^* = 180$ (c,d). (○) Full domain LES; (—) SA-RANS solution; (----) hybrid, LES solution with synthetic turbulence at RANS/LES interface; (-·-) hybrid RANS/LES, synthetic turbulence and forcing at interface.

may occur. The freestream acceleration (from $U_\infty = 1$ to $U_\infty \approx 3$) begins at approximately $100\delta_0^*$ and is completed at $450\delta_0^*$. The case studied here matches the experiments of Warnack and Fernholz (1998).

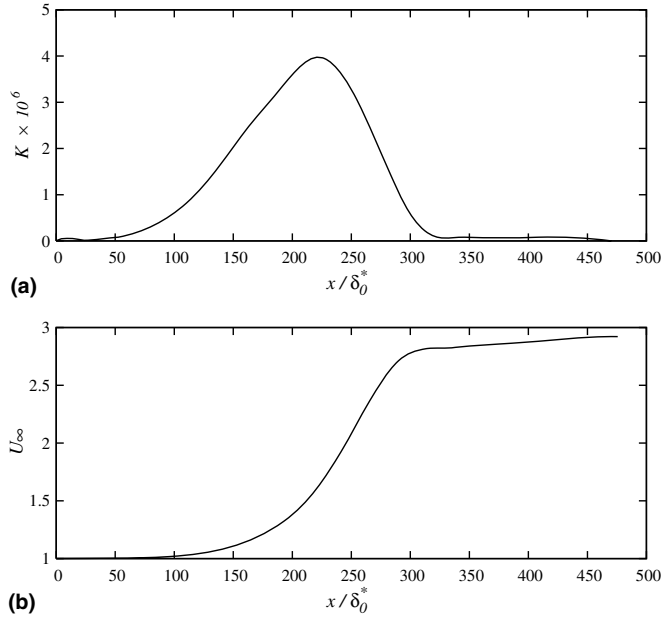

Fig. 4. FPG boundary layer: (a) acceleration parameter K; (b) freestream velocity distribution.

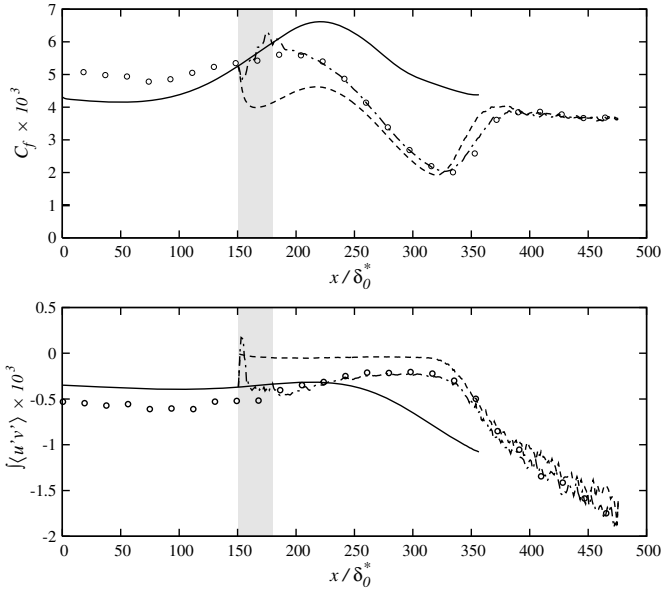

Fig. 5. FPG boundary layer. Coefficient of friction and integrated Reynolds shear stress. (○) Full domain LES; (—) SA-RANS solution; (----) hybrid, LES solution with synthetic turbulence at interface; (-·-) hybrid, LES solution with synthetic turbulence and forcing at the interface. The forcing is applied in the shaded region. RANS/LES interface at $x/\delta_0^* \approx 150$.

The flow acceleration is achieved by imposing a streamwise velocity profile $U_\infty(x)$ at the top boundary of the domain (Lund et al., 1998). Its magnitude was calculated from the acceleration parameter, $K = (\nu/U_\infty^2)(\mathrm{d}U/\mathrm{d}x)$, experimentally obtained by Warnack and Fernholz (1998). The acceleration parameter, K, and the freestream velocity distribution $U_\infty(x)$ are shown in Fig. 4. Since K exceeds the critical value for re-laminarization ($K_{\mathrm{crit}} = 3.5 \times 10^{-6}$) for an extended region of the flow, turbulence is expected to be damped in the region of high acceleration. The flow then re-transitions once the acceleration is removed.

Three simulations were carried out using configurations similar to that shown in Fig. 1. A full-domain LES was first performed using the re-scaling/re-cycling method at an inflow Reynolds number, $Re_{\delta^*} = 1260$. For this simulation

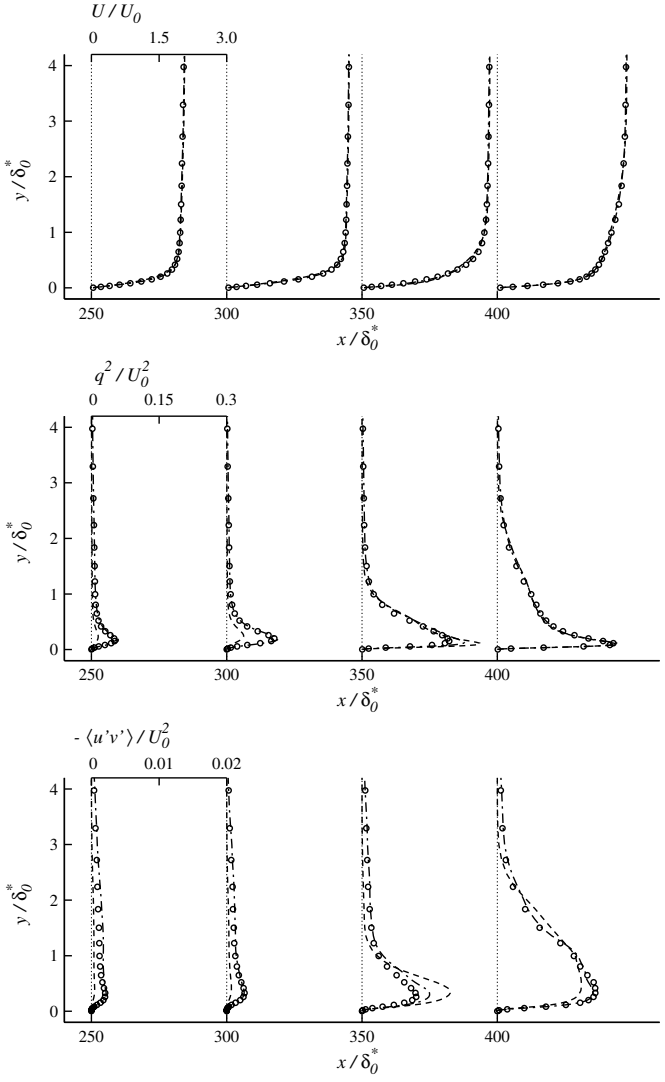

Fig. 6. FPG boundary layer. Profiles of mean velocity, q^2 and Reynolds shear stress at $x/\delta_0^* = 250, 300, 350$ and 400. RANS/LES interface at $x/\delta_0^* \approx 150$. (○) Full domain LES; (—) SA-RANS solution; (---) hybrid, LES solution with synthetic turbulence at interface; (-·-) hybrid, LES solution with synthetic turbulence and forcing at the interface.

the domain length was $476\delta_0^*$, the width was $20\delta_0^*$ and the height was $20\delta_0^*$. A somewhat coarse grid ($512 \times 64 \times 64$) was used, since the comparisons were primarily being made between this full LES and a number of hybrid RANS/LES simulations. Apart from an excessively rapid re-transition, due to the somewhat coarse mesh used, the numerical results are in good agreement with the experiment. See De Prisco et al. (in press) for a validation of the LES data. Two hybrid calculations were performed that included a RANS domain $350\delta_0^*$ long, and an LES region that started at $x/\delta_0^* = 150$ and extended to $476\delta_0^*$ (i.e., had a length $326\delta_0^*$). Synthetic turbulence with and without controlled forcing was introduced at the RANS/LES interface. A second set of hybrid calculations was also carried out in which the RANS/LES interface was placed at $x/\delta_0^* \approx 225$. In the first case, the pressure gradient in the interface region is relatively mild (and the RANS is expected to be accurate). In the second case, modeling errors in the RANS may be more significant; this case, therefore, tests the sensitivity of the hybrid calculation to inaccuracies in the RANS model.

Fig. 5 shows the coefficient of friction and the Reynolds shear stress integrated in the wall-normal direction. In the full-domain LES, C_f initially increases as the FPG is applied and the freestream velocity U_∞ increases. In the high-acceleration region, however, the flow is unable to respond fast enough to the perturbation from equilibrium introduced by the pressure gradient. As a consequence, the burst cycle is disrupted and the flow begins to re-laminarize, as reflected in the decrease of C_f. Once the pressure gradient is removed, the flow quickly re-transitions to a fully turbulent state. These physical phenomena are well-known, and have been observed in experimental (Warnack and Fernholz, 1998) and numerical (Piomelli et al., 2000) studies. Results from the full-domain LES are in fairly good agreement with the experiments, except in the recovery region where the re-transition occurs slightly later in the simulations due to the marginal resolution in this area. Turbulence modeling is incapable of predicting this effect, as shown by the results of the RANS, which extend to the re-laminarization region.

The results of the hybrid simulations are in good agreement with the full-domain LES when forcing is used. By the end of the region where the forcing is applied, both the C_f and the integrated Reynolds stress are in good

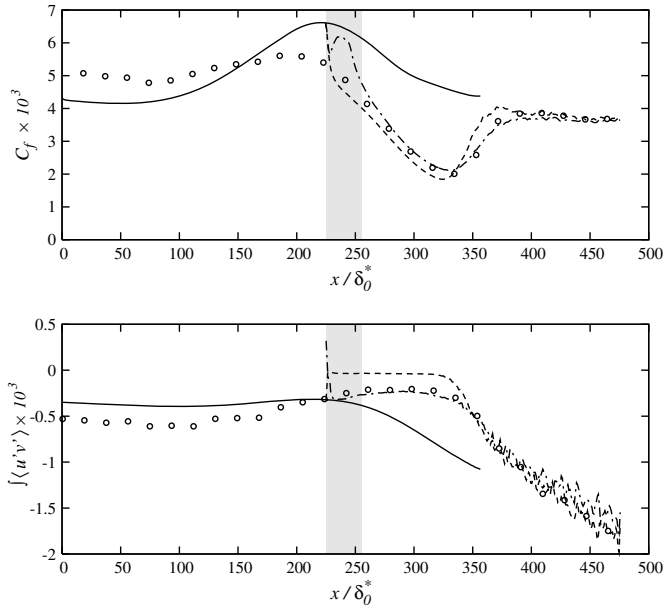

Fig. 7. FPG boundary layer. Coefficient of friction and integrated Reynolds shear stress. (○) Full domain LES; (—) SA-RANS solution; (----) hybrid, LES solution with synthetic turbulence at interface; (-·-) hybrid, LES solution with synthetic turbulence and forcing at the interface. The forcing is applied in the shaded region. RANS/LES interface at $x/\delta_0^* \approx 225$.

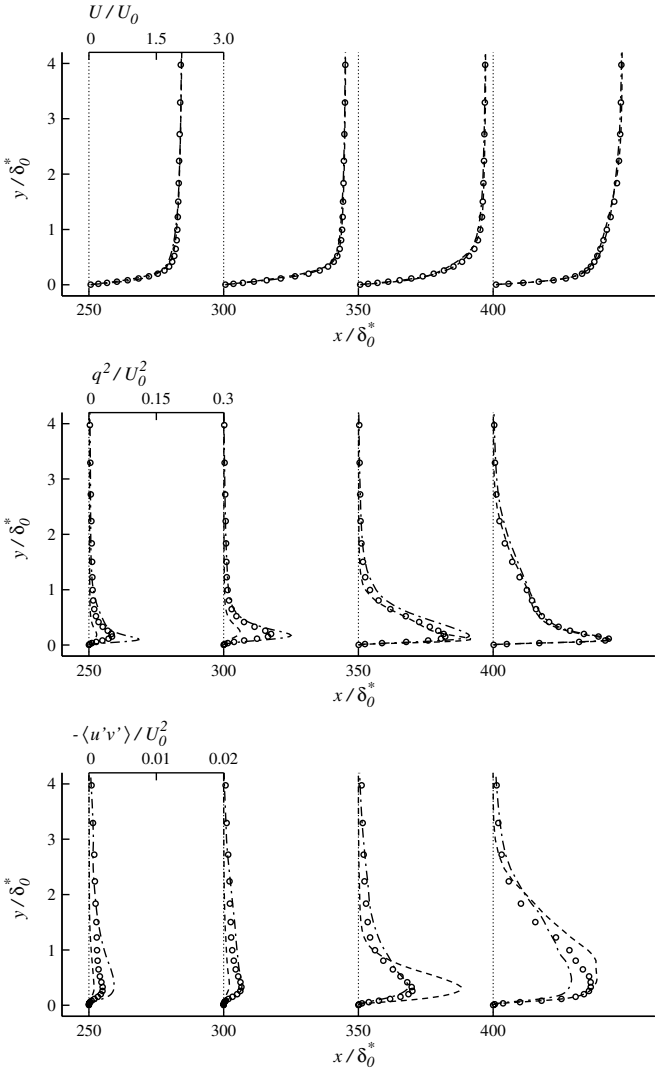

Fig. 8. FPG boundary layer. Coefficient of friction and integrated Reynolds shear stress. (○) Full domain LES; (—) SA-RANS solution; (----) hybrid, LES solution with synthetic turbulence at interface; (-·-) hybrid, LES solution with synthetic turbulence and forcing at the interface. RANS/LES interface at $x/\delta_0^* \approx 225$.

agreement with the target RANS and with the full-domain LES. Synthetic turbulence alone results in an amplification of the flow tendency towards laminarization, and in significant differences with the reference LES.

Mean velocity, q^2 and Reynolds shear stress profiles for these cases are shown in Fig. 6. Without the forcing the q^2 and Reynolds shear stress are significantly under-predicted near the interface ($x/\delta_0^* = 250$ and 300) due to the initial laminarization of the oncoming flow. Due to more rapid re-transition, the simulation without the forcing overpredicts q^2 and the Reynolds shear stress at $x/\delta_0^* = 350$. The hybrid simulation that uses the controlled forcing in the overlap region shows very good agreement with the full-domain LES at the four locations shown.

Results corresponding to the hybrid simulations with the RANS/LES interface at $x/\delta_0^* \approx 225$ are shown in Figs. 7 and 8. Again, due to the laminarization of the oncoming flow, the hybrid simulation without the controlled forcing under-predicts q^2 and the Reynolds shear stress near the interface and shows a much faster transition than the full-domain LES. With the controlled forcing the simulation shows good agreement with the full-domain LES. The agreement is not as good as in the simulation with the RANS/LES interface at $x/\delta_0^* = 150$. This is due to the errors in the RANS model, which result in an incorrect velocity profile and shear-stress distribution at the inflow. The errors due to the RANS calculation, however, do not extend far into the flow: by the end of the forcing region the hybrid calculation results match reasonably well with the full-domain reference case. Notice that the Reynolds shear stress for the hybrid simulation does not match the RANS results in the overlapping region where the controller is active. In this region, because of the strong acceleration of the flow, the controller is unable to drive the shear stress towards to the RANS solution, instead the dynamics of the LES dominate and the solution shows good agreement with the full-domain LES.

Contours of the streamwise velocity in a plane parallel to the wall ($y/\delta_0^* = 0.142$) are shown in Fig. 9 for the full-domain LES and the four hybrid RANS/LES cases.

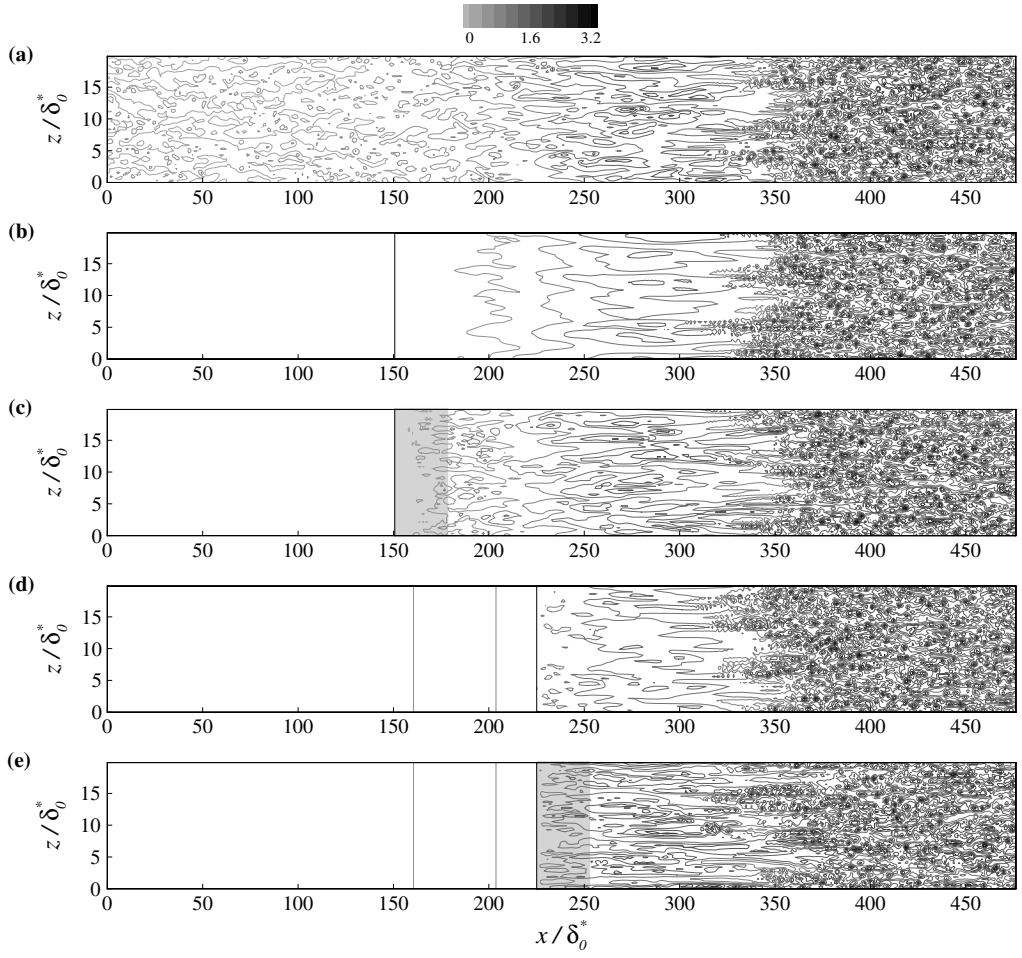

Fig. 9. FPG boundary layer. Contours of the instantaneous streamwise velocity at $y/\delta_0^* = 0.142$. (a) Full-domain LES; (b) hybrid RANS/LES, synthetic turbulence alone, RANS/LES interface at $x/\delta_0^* = 150$; (c) hybrid RANS/LES, synthetic turbulence and controlled forcing, RANS/LES interface at $x/\delta_0^* = 150$; (d) hybrid RANS/LES, synthetic turbulence alone, RANS/LES interface at $x/\delta_0^* = 250$; (e) hybrid RANS/LES, synthetic turbulence and controlled forcing, RANS/LES interface at $x/\delta_0^* = 150$.

The full-domain LES shows features typical of a boundary-layer experiencing a favorable pressure-gradient: the near-wall structures are elongated in the streamwise direction and a re-transition process that mimics bypass-transition follows the removal of the pressure gradient. In both cases in which only synthetic turbulence is used at the RANS/LES interface (Fig. 9b and d), the structures in the FPG region are more coherent and larger than in the full-domain LES, due to the lack of structural information in the upstream boundary layer. When the controlled forcing is used (Fig. 9c and e) this structural information is generated quickly by the control, which is designed to amplify the strongest bursts and ejections. The structures in the FPG region are then in much better agreement with the full-domain LES.

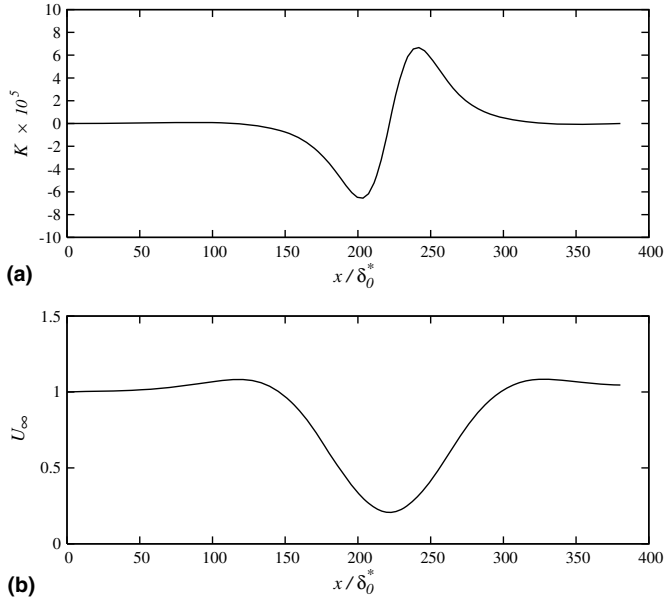

Fig. 10. APG boundary layer: (a) acceleration parameter K; (b) free-stream velocity distribution.

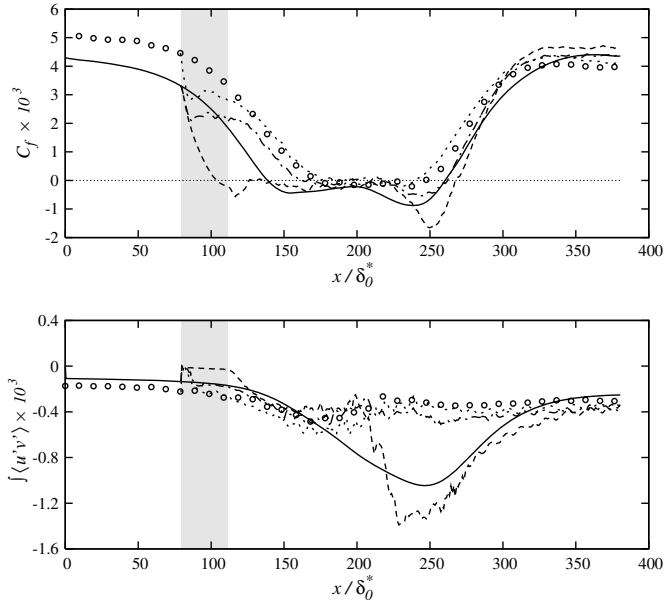

Fig. 11. APG boundary layer. Coefficient of friction and integrated Reynolds shear stress. (○) Full domain LES; (—) SA-RANS solution; (----) hybrid, LES solution with synthetic turbulence at interface; (-·-) hybrid, LES solution with synthetic turbulence and forcing at the interface; (···) hybrid, synthetic turbulence and controlled forcing, LES statistics at the inflow. The forcing is applied in the shaded region.

3.3. Adverse-pressure-gradient boundary layer

Hybrid simulations were next carried out in an adverse-pressure-gradient (APG) boundary-layer that undergoes separation. The configuration of these simulations is similar to that of the DNS by Na and Moin (1998), however at a higher inflow Reynolds number, $Re_{\delta^*} = 1260$. At the top boundary, the same profile of V used by Na and Moin (1998) was imposed. The acceleration parameter and free-stream velocity for this case are shown in Fig. 10. This flow is characterized by a strong adverse pressure-gradient that causes the flow to separate, followed by a strong favorable one that closes the re-circulation bubble.

The computational domain used in the full-domain LES was $360\delta_0^* \times 52\delta_0^* \times 40\delta_0^*$. This LES, which used the re-scaling/re-cycling method at the inflow, used a grid of $512 \times 64 \times 128$. Similar simulations at the same Reynolds number as Na and Moin (1998) showed excellent agreement with the DNS results. The RANS calculations for the hybrid cases were extended to cover the entire flow domain to remove difficulties of placing outflow boundary conditions close to reversed-flow regions. The LES region started at $x/\delta_0^* \approx 80$, and used the RANS data at that location for the synthetic turbulence generation, as well as target for the controlled forcing algorithm.

Fig. 11 shows the C_f and integrated Reynolds shear stress. As the boundary layer is subjected to the adverse pressure-gradient, C_f decreases until the flow separates at $x/\delta_0^* \approx 170$. A weak separation bubble can then be observed in the full-domain LES, which has a length of approximately $80\delta_0^*$. The ensuing favorable pressure-gradient the causes the flow to reattach. The results from the RANS simulation are quite different and show a stronger re-circulation bubble and much larger levels of Reynolds shear stress in the separated region. The differences in the bubble shapes are more apparent in the mean streamlines shown in Fig. 12.

Hybrid simulations were carried out with the RANS/LES interface located at $x/\delta_0^* = 80$. At this location C_f has begun to drop as the adverse pressure-gradient has just begun to affect the boundary layer. Note that at this location, the RANS and full-domain LES results are significantly different: the C_f predicted by the RANS is significantly lower than the LES result. Fig. 11 compares the C_f and integrated Reynolds shear stress of the hybrid simulations with the full-domain LES and RANS simulations. The hybrid simulation with synthetic turbulence only

at the interface initially laminarizes, shows very early separation (at $x/\delta_0^* \approx 100$) and a region of very strong backflow near the downstream edge of the bubble. The resulting separation bubble is shown in Fig. 12(c) and is clearly larger than that predicted by the full-domain LES.

Profiles of mean velocity, q^2 and Reynolds shear stress profiles at several locations are shown in Fig. 13. The shape of the separation bubble has a large influence on the predicted Reynolds shear stress: the larger bubble predicted by the RANS simulation shows much larger levels of Reynolds shear stress in the re-circulation region.

When the controlled forcing is used, the results are in better agreement with the LES. The separation location is only slightly upstream of the full-domain LES, and the strong backflow near the downstream bubble-edge is significantly reduced. The integrated shear stress is also in better agreement with the full-domain LES. However, the mean streamlines shown in Fig. 12(d) show that the separation bubble in this case is still larger than the full-domain LES. This is also observable in the mean velocity, q^2 and Reynolds shear stress profiles shown in Fig. 13.

To separate the errors due to the methods used to generate turbulent eddies from those due to inaccuracies of the RANS model, a further simulation was performed using the time-averaged statistics taken from the full-domain LES at the interface location. Notice that the isotropy assumption (11) was still used when generating the synthetic turbulence, so that any difference is due only to a more accurate prediction of the mean flow and shear stresses. Using these statistics results in much better agreement with the full-domain LES, as shown in Figs. 11–13. This case illustrates how the quality of the RANS solution in a hybrid RANS/LES affects the LES results, especially in separated boundary layer cases in which the shape of the separation bubble is highly dependent on the properties of the upstream boundary layer.

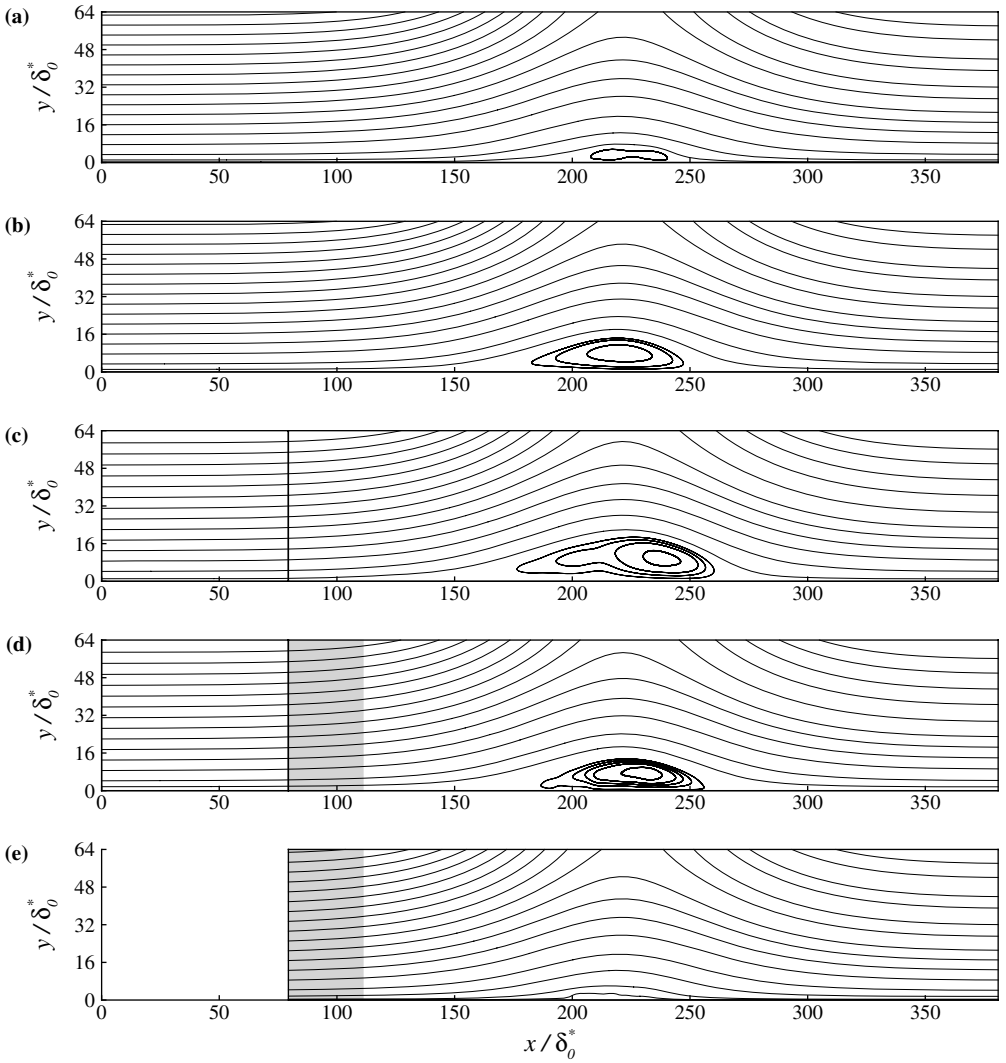

Fig. 12. APG boundary layer. Time-averaged streamlines. (a) Full-domain LES; (b) SA-RANS; (c) hybrid RANS/LES, synthetic turbulence alone; (d) hybrid RANS/LES, synthetic turbulence and controlled forcing; (e) hybrid RANS/LES, synthetic turbulence and controlled forcing, LES statistics at the inflow.

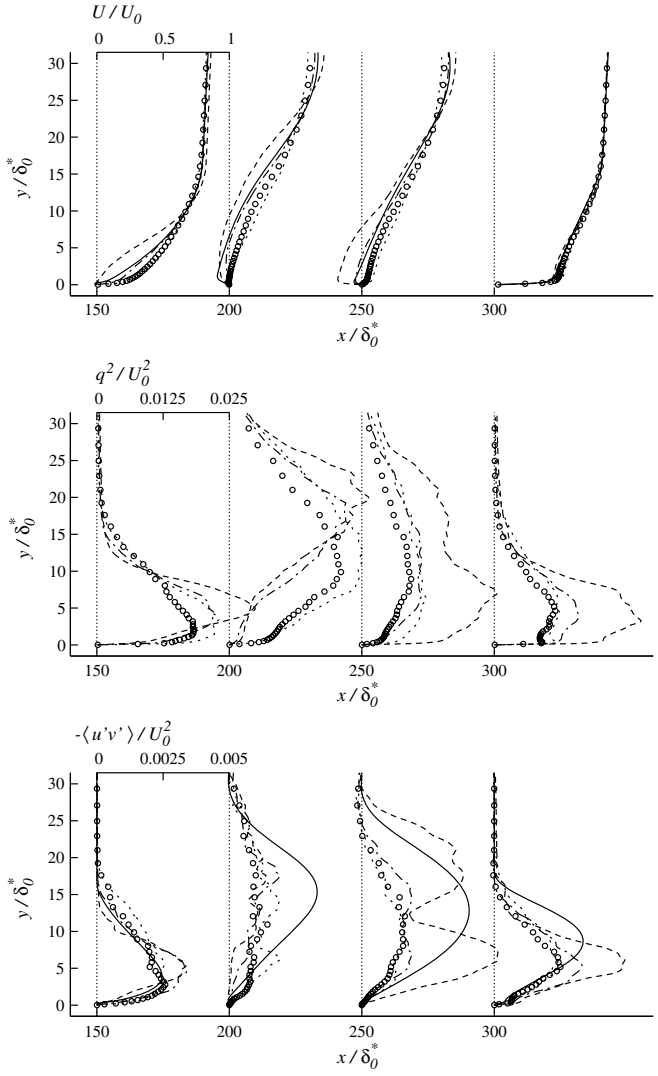

Fig. 13. APG boundary layer: profiles of mean velocity, q^2 and Reynolds shear stress at $x/\delta_0^* = 150, 200, 250$ and 300. (○) Full domain LES; (—) SA-RANS solution; (----) hybrid, LES solution with synthetic turbulence at interface; (-·-) hybrid, LES solution with synthetic turbulence and forcing at the interface; (···) hybrid, synthetic turbulence and controlled forcing, LES statistics at the inflow.

4. Conclusions

Hybrid RANS/LES simulations have been performed using a coupling technique based on a combined synthetic turbulence and controlled forcing method that has been shown to be effective in generating fully developed, realistic turbulence starting from synthetic turbulence within a short distance. In this method, an overlapping region is used in which the RANS solution provides statistics for the synthetic turbulence generation and controlled forcing methods used in the LES region. This method could also be used if the planes obtained from a separate DNS or LES calculation of a similar flow were used in the way proposed, for instance, by Schlüter et al. (2004). Hybrid simulations of zero-pressure gradient, favorable-pressure gradient and adverse-pressure gradient boundary layers were performed, and the results were compared with full-domain LES and RANS results.

In the zero-pressure gradient boundary layer the hybrid simulations using the controlled forcing showed good agreement with a full-domain LES. Using the controlled forcing method, a relatively short transition distance was needed for realistic turbulent to be generated downstream of the RANS/LES interface. Profiles of q^2 showed that in the LES region of the hybrid simulation the slow wall-outward redevelopment of turbulence caused the turbulent kinetic energy in the outer layer of the boundary layer to redevelop slower than the TKE in the inner layer and the mean velocity.

Hybrid simulations were performed of a boundary-layer in a strongly favorable-pressure gradient in which laminarization of the flow has been observed in past experimental (Warnack and Fernholz, 1998) and numerical (Piomelli et al., 2000) studies. A RANS simulation was performed that was unable to capture the retransition of the flow. In the hybrid simulations without the controlled forcing, the decay of turbulence downstream of the RANS/LES interface had a detrimental effect on the predictions of the laminarization and re-transition processes. This initial decay was reversed by the controlled forcing method, and the resulting agreement with the full-domain LES was very good.

Simulations were also performed in an adverse-pressure gradient boundary layer that undergoes separation and reattachment. RANS simulations predicted a separation bubble much larger than the full-domain LES predictions. In the hybrid simulations, the shape of the separation bubble was found to be highly dependent on the properties of the upstream boundary layer. Without the controlled forcing, the turbulence in the LES region downstream of the RANS/LES interface quickly laminarized, causing a very early separation and a large separation bubble. When the controlled forcing was used, the decay was reversed and separation was fairly accurately predicted. However, in this hybrid simulation the shape of the re-circulation bubble more closely matched the RANS simulation than the LES results. Truncated domain LES simulations, using the statistics from the full-domain LES for the synthetic turbulence and controlled forcing methods showed much better agreement with the full-domain LES. This illustrates one of the limitations of hybrid RANS/LES methods, especially in similar cases where the flow in the LES region is highly dependent on the accurate prediction of upstream boundary layer properties, and points out the critical need to place the interface in a region where RANS models are accurate, or to resort to more sophisticated turbulence models.

Overall, a number of successful hybrid RANS/LES simulations of non-equilibrium boundary layers have been carried out. These simulations indicate that proper handling of the RANS/LES interface is critical in obtaining accurate results in LES regions. Using synthetic turbulence at the interface alone the turbulence in the LES region quickly

decays, causing incorrect mean velocity and q^2 profiles. We found that by using an overlapping RANS/LES region, in which a controlled forcing method was used to drive the shear stress in the LES towards values obtained from RANS, this initial decay could be quickly reversed and the hybrid simulations were in good agreement with full-domain LES.

We next plan to perform simulations of the more challenging case of flow over an airfoil. Here, we plan to use two-dimensional flow solvers with RANS models in the laminar and zero-pressure gradient regions, while transitioning to a three-dimensional LES in the adverse-pressure gradient and wake regions at the rear of the airfoil. We are also investigating generalizations of the forcing method that take into account the more complex shear-stress production mechanisms that occur in complex three-dimensional flows.

Acknowledgements

Effort sponsored by the Air Force Office of Scientific Research, Air Force Materiel Command, USAF, under grant number F49620-03-1-0112, monitored by Dr. T. Beutner and Lt. Col. R. Jefferies. The US Government is authorized to reproduce and distribute reprints for Governmental purposes notwithstanding any copyright notation thereon. The views and conclusions contained herein are those of the authors and should not be interpreted as necessarily representing the official policies or endorsements, either expressed or implied, of the Air Force Office of Scientific Research or the US Government. The authors also wish to thank Dr. Elias Balaras for helpful discussions.

References

Batten, P., Goldberg, U., Chakravarthy, S., 2004. Interfacing statistical turbulence closures with large-eddy simulation. AIAA J. 42 (3), 485–492.

Bradshaw, P., Ferriss, D.H., Atwell, N.P., 1967. Calculation of boundary layer development using the turbulent energy equation. J. Fluid Mech. 23, 31–64.

De Prisco, G., Keating, A., Piomelli, U., Balaras, E., in press. Large-eddy simulation of accelerating boundary layers. In: Oberlack, M., Guenther, S., Weller, T., Khujadze, G., Osman, A., Frewer, M., Peinke, J. (Eds.), Progress in Turbulence, vol. 2. Springer, Berlin.

Germano, M., Piomelli, U., Moin, P., Cabot, W., 1991. A dynamic subgrid-scale eddy viscosity model. Phys. Fluids A 3, 1760–1765.

Keating, A., Piomelli, U., 2004. Synthetic generation of inflow velocities for large-eddy simulations. AIAA Paper, 2004–2547.

Keating, A., Piomelli, U., Balaras, E., Kaltenbach, H.-J., 2004. A priori and a posteriori tests of inflow conditions for large-eddy simulation. Phys. Fluids 16 (12), 4696–4712.

Kim, J., Moin, P., 1984. Application of a fractional step method to incompressible Navier–Stokes equations. J. Comput. Phys. 59 (2), 308–323.

Kraichnan, R.H., 1970. Diffusion by a random velocity field. Phys. Fluids 13 (1), 22–31.

Le, H., Moin, P., Kim, J., 1997. Direct numerical simulation of turbulent flow over a backward-facing step. J. Fluid Mech. 330, 349–374.

Lund, T.S., Wu, X., Squires, K.D., 1998. Generation of inflow data for spatially-developing boundary layer simulations. J. Comput. Phys. 140, 233–258.

Meneveau, C., Lund, T.S., Cabot, W.H., 1996. A Lagrangian dynamic subgrid-scale model of turbulence. J. Fluid Mech. 319, 353–385.

Menter, F.R., 1997. Eddy viscosity transport equations and their relation to the k–ϵ model. J. Fluids Eng. 119, 876–884.

Na, Y., Moin, P., 1998. Direct numerical simulation of a separated turbulent boundary layer. J. Fluid Mech. 374, 379–405.

Piomelli, U., Balaras, E., Pascarelli, A., 2000. Turbulent structures in accelerating boundary layers. J. Turbulence 1, 001.

Schlüter, J.U., Pitsch, H., Moin, P., 2004. LES inflow conditions for coupling with Reynolds-averaged flow solvers. AIAA J. 42, 478–484.

Smirnov, A., Shi, S., Celik, I., 2001. Random flow generation technique for large eddy simulations and particle-dynamics modeling. J. Fluids Eng. 123, 359–371.

Spalart, P.R., Allmaras, S.R., 1994. A one-equation turbulence model for aerodynamics flows. La Recherche Aérospatiale 1, 5–21.

Spalart, P.R., Jou, W.H., Strelets, M., Allmaras, S.R., 1997. Comments on the feasibility of LES for wings, and on a hybrid RANS/LES approach. In: Liu, C., Liu, Z. (Eds.), Advances in DNS/LES. Greyden, Columbus, OH, pp. 137–148.

Spille-Kohoff, A., Kaltenbach, H.-J., 2001. Generation of turbulent inflow data with a prescribed shear-stress profile, Third AFOSR International Conference on DNS/LES, Arlington, TX, 5-9, August, 2001. In: Liu, C., Sakell, L., Beutner, T. (Eds.), DNS/LES Progress and Challenges. Greyden, Columbus, OH.

Squires, K.D., 2004. Detached-eddy simulation: current status and perspectives. In: Friedrich, R., Geurts, B.J., Métais, O. (Eds.), Direct and Large-Eddy Simulation V. Kluwer, Dordrecht, pp. 465–480.

Townsend, A.A., 1962. Equilibrium layers and wall turbulence. J. Fluid Mech. 11, 97–120.

Warnack, D., Fernholz, H.H., 1998. The effects of a favourable pressure gradient and of Reynolds number on an incompressible axisymmetric turbulent boundary layer. Part 2. The boundary layer with relaminarization. J. Fluid Mech. 359, 357–381.